AIP | Review of Scientific Instruments

Model based control of dynamic atomic force microscope

Chibum Lee and Srinivasa M. Salapaka

Citation: Review of Scientific Instruments **86**, 043703 (2015); doi: 10.1063/1.4917301
View online: http://dx.doi.org/10.1063/1.4917301
View Table of Contents: http://scitation.aip.org/content/aip/journal/rsi/86/4?ver=pdfcov
Published by the AIP Publishing

Model based control of dynamic atomic force microscope

Chibum Lee[1] and Srinivasa M. Salapaka[2,a)]
[1]*Department of Mechanical System Design Engineering, Seoul National University of Science and Technology, Seoul 139-743, South Korea*
[2]*Department of Mechanical Science and Engineering, University of Illinois at Urbana-Champaign, Urbana, Illinois 61801, USA*

(Received 12 December 2014; accepted 30 March 2015; published online 23 April 2015)

A model-based robust control approach is proposed that significantly improves imaging bandwidth for the dynamic mode atomic force microscopy. A model for cantilever oscillation amplitude and phase dynamics is derived and used for the control design. In particular, the control design is based on a linearized model and robust H_∞ control theory. This design yields a significant improvement when compared to the conventional proportional-integral designs and verified by experiments. © *2015 AIP Publishing LLC.* [http://dx.doi.org/10.1063/1.4917301]

I. INTRODUCTION

Since atomic force microscope (AFM) was invented in 1986,[1] it has evolved into a very versatile and widely used tool for imaging topography as well as measurement of micro-structural parameters with nano-scale resolution.

A schematic of an AFM that demonstrates its working principle is shown in Figure 1. The main probe of an AFM is a micro-cantilever that is soft enough to deflect due to interactive forces between the atoms on the sample and the atoms on the tip. The cantilever deflections are registered by a laser incident on the cantilever, which reflects onto a photo-diode. Difference between the readings from the top and the bottom cells gives a measurement proportional to the cantilever's normal deflection. The measured deflection signal is used to design a feedback control that moves the piezo-positioner vertically in order to compensate for the effect of topographical features of the sample on the cantilever tip. Depending on the sample and intended applications, various modes are obtained by appropriate actuation strategies. In the static mode operation, the tip scans the sample in contact with the surface. If the measured deflection is different from the set point value, the feedback controller applies a voltage signal to extract or retract the vertical piezo to keep the deflection constant. In the dynamic mode operation, the cantilever is externally oscillated at frequency close to its resonance frequency or a harmonic by forcing the base that supports the cantilever with a dither piezo. The cantilever oscillations vary when it interacts with the features on the sample. Thus, the changes in amplitude and phase angle of the cantilever oscillations are indicative of the effects of the tip-sample interaction forces and can be used to infer sample properties including sample topography. The dynamic-mode amplitude modulation AFM with intermittent contact is commonly used for the characterization of various materials in ambient condition including imaging since the cantilever is gentle on the sample and does not damage the sample. The disadvantage of this mode is the slow imaging speed, because the sample-topography data are interpreted from the steady state amplitude values of the cantilever deflection in existing methods. The high frequency excitation with intermittent contact raises a complication in cantilever dynamics.

Although the dynamics and their simplifications have been modeled and analyzed using various theoretical models,[2–5] the models have not been used in designing the control. In the field of control approach in dynamic AFM, a switching of proportional-integral-differential (PID) controllers was proposed based on the probe-loss detection in dynamic mode operation to reduce probe-loss affected regions in an image[6,7] and a new method for better imaging bandwidth through alternative signal was proposed.[8]

In this study, the model based control is applied to improve the performance of dynamic AFM. The paper is organized as follows: In Secs. II and III, dynamic AFM is interpreted in a system engineering view point and a model for the cantilever deflection dynamics is derived. In Sec. IV, averaging techniques are used to derive amplitude-phase dynamics from the deflection dynamics and then the resulting model is linearized. The modeling uncertainties due to the nonlinear effects are also characterized. In Sec. V, a model based controller was designed based on the simplified model with robust $\mathcal{H}_\infty$ control theory. The experimental results are shown in Sec. VI, and the main observations of this study are summarized in Sec. VII.

II. DYNAMIC AFM IN SYSTEM ENGINEERING PERSPECTIVE

To interpret the operating principle in system engineering perspective, the block diagram schematic of an imaging in dynamic AFM is introduced in Figure 2, which excludes the $x-y$ positioning system. The controller, the vertical piezo positioner, the cantilever dynamics model which includes the tip-sample interaction force, and the signal conditioner are represented by K, G_p, $\mathcal{F}$, and Q, respectively. The controller K is designed to regulate the difference e between an amplitude or phase signal y of the deflection signal p and the set point r to zero to compensate the effects of the sample

a)Electronic mail: salapaka@illinois.edu.

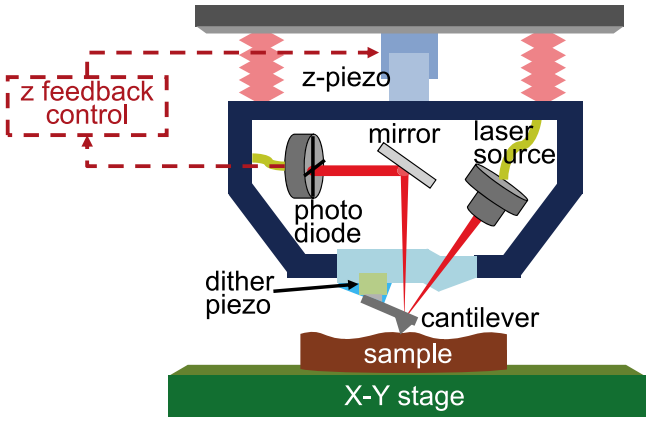

FIG. 1. Schematic of an atomic force microscope.

topography h. The deflection p is described by a nonlinear dynamic model $\mathcal{F}$. The deflection p is the outcome from the forcing of the cantilever, the dither piezo excitation g, the thermal noise η, and the tip-sample interaction force F_{ts} that depends on the sample-position v by vertical piezo actuator and the sample height h.

In amplitude modulation AFM, the dither piezo is oscillated at a frequency ω close to the cantilever resonance frequency ω_r, (i.e., $g(t) = g_0\cos(\omega t)$), and the amplitude of the cantilever deflection p_m is regulated at a constant value. If the sample height h changes during scanning, the amplitude of cantilever deflection also changes after intermittent contact during oscillation. The control signal u gives a measure of the topography h since the sample position v compensates for the effects of h to regulate the amplitude of the deflection signal. In fact, the control signal u from force regulation technique forms the topography signal in most existing imaging AFMs.

III. MODELING OF CANTILEVER AND TIP-SAMPLE INTERACTION

The modeling $\mathcal{F}(g,v,h,\eta)$ which includes the cantilever dynamics and the tip-sample interaction is crucial in analyzing dynamic response of dynamic AFMs.

A single-mode cantilever model which simplifies continuous beam equation is shown to be sufficient for most applications in conventional dynamic mode operation in air or vacuum where the excitation frequency is near the resonance of the first eigenmode[9] and is given by

$$\ddot{p} + \frac{\omega_n}{Q}\dot{p} + \omega_n^2 p = \frac{1}{m}[F_{ts} + F_{ext} + F_{th}], \tag{1}$$

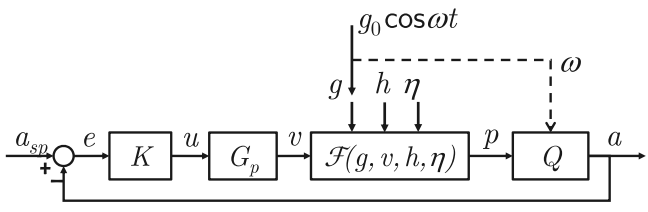

FIG. 2. A block diagram schematic of a dynamic AFM.

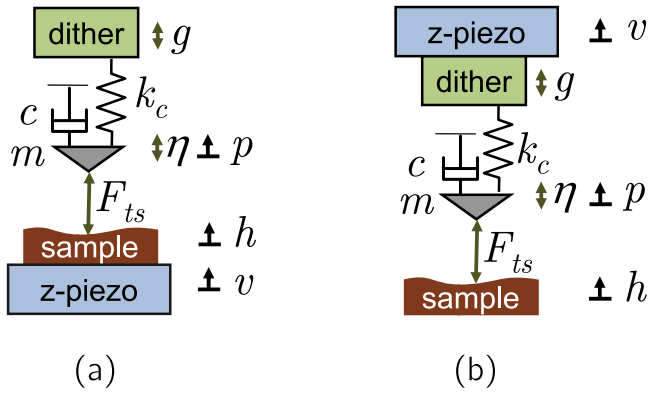

FIG. 3. Single-mode point mass cantilever model with vertical piezo motion.

where ω_n is the first modal frequency, and m is the effective mass of the cantilever and the tip. The force acting on the cantilever includes the tip-sample interaction F_{ts}, the thermal excitation F_{th}, and the excitation from dither piezo F_{ext}. Q represents the associated quality factor given by $Q = \frac{\sqrt{mk_c}}{c} = \frac{1}{2\zeta}$, where ζ is the damping coefficient.

Closed-loop operation of AFMs moves the vertical piezo-actuator to maintain tip-sample interaction at a constant value. The important main concern required for modeling $\mathcal{F}(g,v,h,\eta)$ is the location of vertical piezo-actuator. In the vertical positioning on sample case in Figure 3(a), the tip-sample interaction force F_{ts} is affected by vertical-piezo motion and (1) becomes

$$\ddot{p} + \frac{\omega_n}{Q}\dot{p} + \omega_n^2 p = \frac{1}{m}[F_{ts}(p-h-v) + F_{ext} + F_{th}]. \tag{2}$$

In the prevalent case where the vertical piezo-actuation is on top of the cantilever as shown in Figure 3(b), the vertical-piezo movement changes the cantilever base position and (1) becomes

$$\ddot{p} + \frac{\omega_n}{Q}\dot{p} + \omega_n^2 (p-v) = \frac{1}{m}[F_{ts}(p-h) + F_{ext} + F_{th}]. \tag{3}$$

Since the photo-diode is located in the same inertial frame with base of cantilever, the measurement corresponds to $p^* = p - v$ and the equation about p^* becomes similar to (2) with the assumption of relatively small $\dot{v}$, v compared to cantilever oscillation.[10]

The interaction force between the tip and the sample can be explained by Hertz, Derjaguin-Müller-Toporov (DMT), Johnson-Kendall-Roberts (JKR), and Maugis models.[11,12] This approach can accommodate any tip-sample interaction model; in this study, we present the DMT model, which includes the van der Waals along with Hertz contact force models, since it describes well our experimental setup. This model has also been validated in the literature for dynamic AFM analysis.[13,14] It is particularly relevant to tips with small curvature radius and high stiffness under dry conditions and best suited to our experimental apparatus described in Sec. IV. It is given by

$$F_{ts}(z) = \begin{cases} -\dfrac{HR}{6z^2}, & \text{if } z > a_0 \\ -\dfrac{HR}{6a_0^2} + \dfrac{4}{3}E^*\sqrt{R}(a_0 - z)^{\frac{3}{2}}, & \text{if } z \le a_0 \end{cases}, \tag{4}$$

where z is the separation between tip and sample, H is the Hamaker constant, R is the radius of the tip, $E^* = [\frac{1-\nu_{tip}^2}{E_{tip}} + \frac{1-\nu_{sample}^2}{E_{sample}}]^{-1}$ is the effective Young's modulus, and a_0 is the intermolecular distance. Note that the control design approach described below is valid for any tip-sample interaction model, even though we apply it to the DMT model in the following.

IV. SIMPLIFICATION OF MODEL

A. Asymptotic perturbation methods

The analysis of the dynamic-mode AFM is particularly challenging because the tip traverses a long range of highly nonlinear tip sample interaction potential. The complexity of the dynamics is demonstrated by the experimental and theoretical studies that confirm the existence of chaotic behavior under certain operating conditions.[15,16] The asymptotic perturbation theory has been used to derive and explain the effects of the nonlinear dynamics of the amplitude and phase of the cantilever oscillations, such as the bistability, for the cases when there is *no* vertical piezo-actuation $v = 0$.[13,14,17,18]

In this study, we used the Krylov-Bogoliubov-Mitropolskii (KBM) method[19,20] to derive the amplitude-phase dynamics for the case when there *exists* the vertical piezo-actuation described in (2). For a non-autonomous system with periodic excitation, the second order dynamic equation is given by

$$\ddot{x}(t) + \omega_n^2 x(t) = \epsilon \tilde{f}(x, \frac{dx}{dt}, \omega t). \tag{5}$$

The KBM method assumes a solution of the form

$$x(t) = a\cos\psi + \sum_{i=1}^{\infty} \epsilon^i u_i(A, \psi, \omega t), \tag{6}$$

where $u_i(a, \psi, \omega t)$ is a periodic function of amplitude a, phase ψ, and excitation frequency ω with the period of $T = 2\pi$. For such a system if the harmonic excitation is $\tilde{f}(x, \frac{dx}{dt}, \omega t) = f(x, \frac{dx}{dt}) + E\cos(\omega t)$, where $\omega \approx \omega_n$, then $a - \psi$ dynamics are described by

$$\begin{aligned}
\frac{da}{dt} &= -\frac{\epsilon}{2\pi\omega}\int_0^{2\pi} f(a\cos\theta, -a\omega\sin\theta)\sin\theta d\theta - \frac{\epsilon E}{2\omega}\sin\phi,\\
\frac{d\phi}{dt} &= \omega_n - \omega - \frac{\epsilon}{2\pi\omega A}\int_0^{2\pi} f(a\cos\theta, -a\omega\sin\theta)\cos\theta d\theta\\
&\quad - \frac{\epsilon E}{2\omega A}\cos\phi,
\end{aligned} \tag{7}$$

where $\phi = \psi - \omega_n t$ and a first order dependence ($i = 1$) is assumed in (6).

Note that nonlinear system (2) when non-dimensionalized with $\tau := \omega_n t$ and $\Omega := \frac{\omega}{\omega_n}$ can be written in the form given by (5) and (6) suited for the KBM method as[21]

$$\begin{aligned}
\frac{d^2p}{d\tau^2} + p &= \frac{1}{m\omega_n^2}F_{ts}(p - h - v) - 2\zeta\frac{dp}{d\tau} + \eta + g_0\cos\Omega\tau\\
&= \epsilon f(p, \frac{dp}{d\tau}) + \epsilon E\cos\Omega\tau,
\end{aligned} \tag{8}$$

where $\frac{1}{m}F_{ext} =: g_0\cos\omega t$, $\eta := \frac{1}{m}F_{th}$, $E := \frac{g_0}{\epsilon}$, and $f(p, \frac{dp}{d\tau}) := \frac{1}{\epsilon}[\frac{1}{\omega_n^2 m}F_{ts}(p - h - v) - 2\zeta\frac{dp}{d\tau} + \eta]$. The assumption of small ϵ holds due to the small excitation g_0 in the cantilever support compared to the amplitude of the tip, the large resonance frequency ω_n, the very small damping ζ, and the small thermal noise η. An implicit assumption here is that $h + v$ is constant, which is commonly accepted in perturbation theory, and the time-scale separation between the fast dither dynamics and relatively slow actuation dynamics (on the order of 5% of the cantilever resonance frequency) justifies this assumption.

The KBM method when applied to (8) with the first order approximation results in

$$\begin{aligned}
\frac{da}{dt} &= -\zeta\omega_n a - \frac{\omega_n^2 g_0}{2\omega}\sin\phi,\\
\frac{d\phi}{dt} &= \omega_n - \omega - \frac{1}{2\pi\omega m a}\int_0^{2\pi} F_{ts}(a\cos\theta - h - v)\cos\theta d\theta\\
&\quad - \frac{\omega_n^2 g_0}{2\omega a}\cos\phi,
\end{aligned} \tag{9}$$

where a and ϕ are the amplitude and the phase of cantilever tip p.[10] New model (9) can correspond to $\mathcal{F}$ and Q in Figure 2.

B. Linearized model with uncertainty

For developing model based control, new model (9) requires to be even further simplified since it involves the integration of exogenous input v. The average tip-sample interaction over one cycle of oscillation[4] is given by

$$F_{avg} := \int_0^{2\pi} F_{ts}(a\cos\theta - h - v)\cos\theta d\theta \tag{10}$$

and is a function of the amplitude a and the tip-sample distance $\delta := h + v$. This average force value can be numerically computed. As an example for the silicon microcantilever tip and the silicon oxide sample with the parameters for DMT model in Table I, the average force is shown in Figure 4. The average force F_{avg} can be obtained with respect to the amplitude a and the tip-sample distance δ. In amplitude modulation mode, the set point of amplitude a_{sp} becomes the equilibrium amplitude a_{eq} of the dynamics described by (9). The values at equilibrium (δ_{eq}, ϕ_{eq}) can be obtained from (9) and the nonlinear model is linearized about this point.

Once a linearized model of F_{avg} is obtained, the blocks $\mathcal{F}$ and Q in Figure 2 can be replaced by a single block G_c where the sample height h is an *external disturbance* (input) signal. Figure 5 shows the corresponding new block diagram. If we define the state variables $x_1 = a - a_{eq}$, $x_2 = \phi - \phi_{eq}$ and the input variable $u = \delta - \delta_{eq}$, then the linearized system G_c is given by

TABLE I. Constants and properties of the silicon micro-cantilever tip and silicon oxide sample.

Description	Value
Hamaker constant (Si-SiO_2)	$H = 6.4 \times 10^{-20}$ J
Cantilever tip radius	$R = 10$ nm
Effective elastic modulus	$E^* = 50$ GPa
Intermolecular distance	$a_0 = 0.16$ nm

$$\begin{aligned} \dot{x} &= Ax + Bu, \\ y &= \begin{bmatrix} 1 & 0 \end{bmatrix} x, \end{aligned} \tag{11}$$

where

$$A = \begin{bmatrix} -\zeta\omega_n & -\frac{\omega_n^2 g_0}{2\omega}\cos\phi \\ \frac{F_{avg}(a,\delta)}{2\pi\omega m a^2} - \frac{1}{2\pi\omega m a}\frac{\partial F_{avg}}{\partial a} + \frac{\omega_n^2 g_0}{2\omega a^2}\cos\phi & \frac{\omega_n^2 g_0}{2\omega a}\sin\phi \end{bmatrix}_{(a_{eq},\phi_{eq},\delta_{eq})},$$

$$B = \begin{bmatrix} 0 \\ -\frac{1}{2\pi\omega m a}\frac{\partial F_{avg}}{\partial \delta} \end{bmatrix}_{(a_{eq},\phi_{eq},\delta_{eq})}.$$

Partial derivatives of average force can be obtained numerically.

V. ROBUST $\mathcal{H}_\infty$ CONTROL

Our approach is to use the linearized model for designing the control v to achieve large imaging bandwidth while ensuring robustness to modeling uncertainties arising from the nonlinear effects. Since F_{avg}, $\frac{\partial F_{avg}}{\partial a}$, and $\frac{\partial F_{avg}}{\partial \delta}$ can vary during scanning due to changes in the amplitude a and the separation δ. Accordingly, the cantilever model $G_c(s)$ is modeled to be in a set as follows:

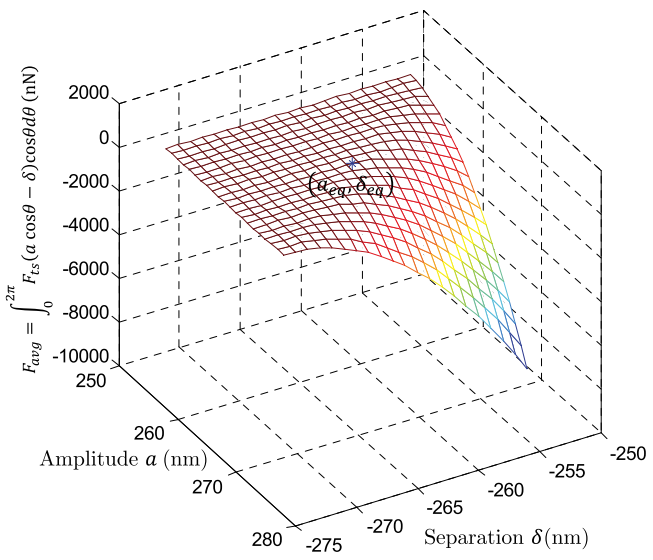

FIG. 4. Average force $F_{avg} = \int_0^{2\pi} \frac{1}{m} F_{ts}(a\cos\theta - h - v)\cos\theta d\theta$ for the case with Table I.

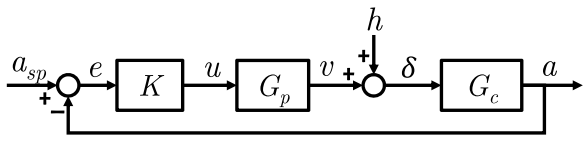

FIG. 5. A new block diagram for model based control of dynamic AFM.

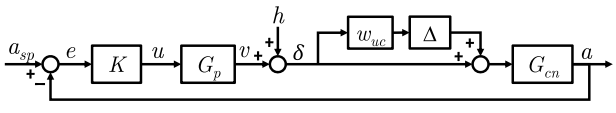

FIG. 6. A block diagram schematic with multiplicative uncertainty.

$$G_c(s) = G_{cn}(1 + w_{uc}(s)\Delta(s)),\ |\Delta(j\omega)| \le 1 \forall \omega, \tag{12}$$

where $w_{uc}(s)\Delta(j\omega)$ represents the modeling uncertainties. After inclusion of the uncertainty block, Figure 5 can be modified to Figure 6.

For robust stability with multiplicative uncertainty in (12), the necessary and sufficient condition is given by $|T| < 1/|w_{uc}|$ for all ω,[22] where $T = G_c G_p K/(1 + G_c G_p K)$ is the complementary sensitivity transfer function. The tracking error (see Figure 5) is given by $e_{tr} = a_{sp} - a = Sa_{sp} - SG_c h$ and the estimation error is given by $e_{est} = h + v = G_p K S a_{sp} + Sh$ where the sensitivity transfer function $S = 1/(1 + G_c G_p K)$. Thus, the control objective for performance is to reduce the tracking and estimation errors small by making SG_c and S small. Since a_{sp} is constant and the dc gain of S is very small, the tracking and estimation errors from a_{sp} are negligible. The topography change h can be estimated with high fidelity if the sensitivity transfer function S is very small in the frequency range where h has dominant components. The sensitivity transfer function S can be shaped with the weighting function w_s such that $\|w_s(s)S(s)\|_\infty < 1$.

The robust performance condition is given by

$$\max(|w_s S| + |w_{uc} T|) < 1 \qquad \text{for all } \omega, \tag{13}$$

which means the performance (low tracking error) is satisfied for all possible plants. The general framework for this problem can be given as Figure 7 and the robust controller can be designed using $\mathcal{H}_\infty$ stacked synthesis method.[22]

VI. VERIFICATION

The model for dynamic-mode AFM and the control design were, respectively, verified and demonstrated on an AFM (MFP-3D, Asylum Research, Inc.). In the experiments, a cantilever with silicon tip (AC240TS, Olympus, Inc.) and a silicon oxide calibration grating (NGR22010, Veeco Metrology, Inc.) were used as the probe and the sample, respectively. The control logic was implemented on a digital signal processor DSP card (TMS320C6713 from Texas Instruments, Inc.).

The spring constant, resonance frequency, and damping ratio of the cantilever are experimentally obtained from thermal excitation and sweeping test as $k = 2.66$ nn/V,

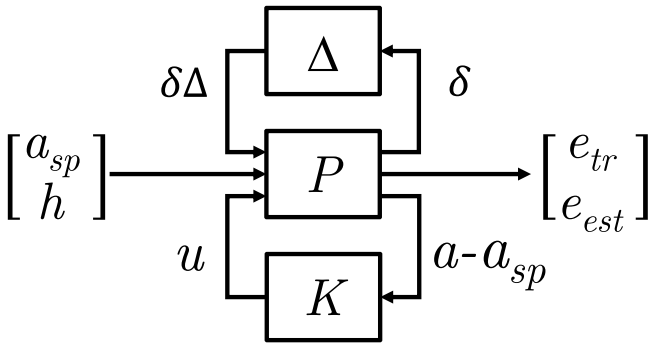

FIG. 7. A general framework for robust control optimization.

$f_r = 82.274$ kHz, and $\zeta = 2.7964 \times 10^{-3}$. In scanning, the amplitude was set as $a_{sp} = a_{eq} = 262.22$ nm which was 80% of amplitude in the air.

A. KBM method on cantilever and tip-sample interaction

For verifying the averaging method in cantilever and tip-sample interaction, an arbitrary sample-profile h was given and the deflection signal $p(t)$ determined from (3), and compared the amplitude signal $a(t)$ and phase signal $\phi(t)$ as determined from the KBM method in (9) with $v = 0$. Amplitude and phase dynamics obtained from KBM methods show a good match with dynamics of the cantilever deflection signal p for slow varying sample height as shown in Figure 8.

B. Experimental result of robust $\mathcal{H}_\infty$ control

To find the vertical piezo-actuator dynamic model, the frequency-response based identification was done using an HP 35670A dynamic analyzer. A sine-sweep over from 1 Hz to 10 kHz was given to piezo-actuator and the signal from built-in position sensor was analyzed while the cantilever is in air. The obtained linear model is given by

$$G_p(s) = \frac{-6.698 \times 10^{-5}(s + 5.24 \times 10^4)(s - 2.817 \times 10^4)}{(s + 6911)(s^2 + 1359s + 1.975 \times 10^8)}, \tag{14}$$

with the unit of m/V. Note that the nonlinear effects such as hysteresis and creep of piezo-actuators[23,24] can be accommodated as modeling uncertainties in the control design.[25]

For the set-point amplitude $a_{sp} = a_{eq} = 262.22$ nm, the equilibrium values from (9) were obtained by $\delta_{eq} = -261.81$ nm, and $\phi_{eq} = -49.40°$. The nominal plant obtained from linearization (11) is given by

$$G_{cn}(s) = \frac{-2.843 \times 10^{15}}{s^2 + 2891s + 9.347 \times 10^8} \tag{15}$$

in unit of V/m.

F_{avg}, $\frac{\partial F_{avg}}{\partial a}$, and $\frac{\partial F_{avg}}{\partial \delta}$ are assumed to have uncertainties with the bound of 20% of nominal value. The set of perturbed plants $G_c(s)$ is shown in Figure 9(a). To find the uncertainty bound, $|\frac{G_c(s) - G_{cn}(s)}{G_{cn}(s)}|$ and its upper bound $w_{uc}(s)$ are shown in Figure 9(b). The original bound was set to the second order but with consideration of high frequency noise attenuation and low order, the modified bound is given by

$$w_{uc}(s) = \frac{s + 2961}{0.1s + 5922}. \tag{16}$$

The weighting function for S is selected as

$$w_s(s) = \frac{0.5s + 592.2}{s + 5.922}. \tag{17}$$

The resulting controller from $\mathcal{H}_\infty$ stacked synthesis method is given by

$$K_\infty(s) = \frac{-666\,190(s + 59\,218)(s + 6911)}{(s + 5.922)(s + 59\,241)(s + 12\,080)} \times \frac{(s^2 + 1359s + 1.975 \times 10^8)(s^2 + 2891s + 9.347 \times 10^8)}{(s^2 + 39\,130s + 6.309 \times 10^8)(s^2 + 13\,980s + 1.321 \times 10^9)}. \tag{18}$$

The cost $\||w_s S| + |w_{uc} T|\|_\infty$ is bounded by 0.91. The results are shown in Figure 10. The order of the controller $K_\infty(s)$ in (18) is reduced to 6 and discretized for implementation.

The results of imaging were compared with conventional proportional-integral (PI) controller. An aggressive PI controller was designed which is almost marginally stable with higher bandwidth compared to default PI controller used

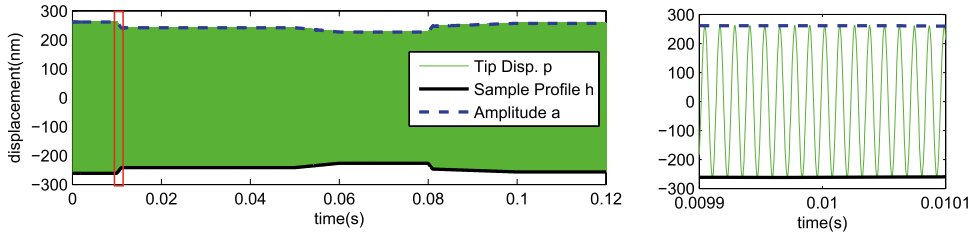

FIG. 8. Comparison of original and KBM dynamics for slow varying height. The cantilever deflection $p(t)$ (solid green) is from (3), and the amplitude signal (dashed blue) is $a(t)$ derived from (9). The plot on the right side is an expanded view of the red section in the left plot.

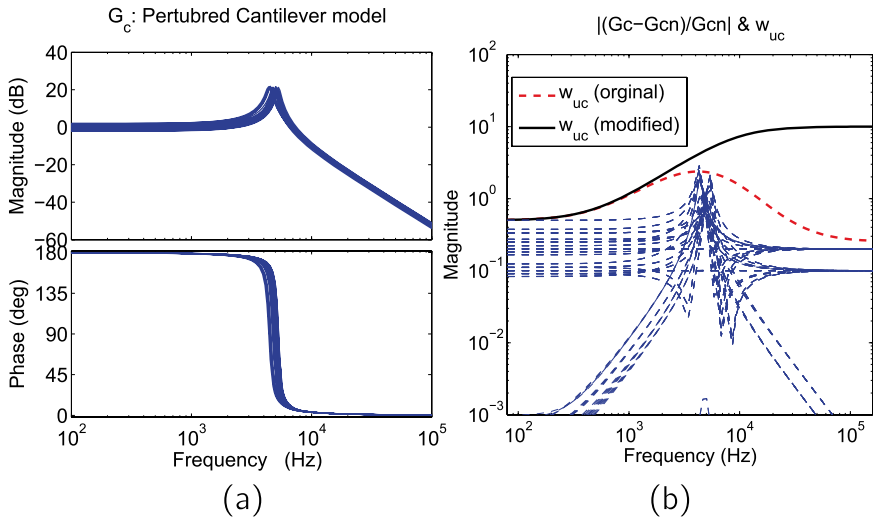

FIG. 9. (a) Perturbed plant $G_{cn}(1+w_{uc}(s)\Delta(s))$ (b) $|\frac{G_c(s)-G_{cn}(s)}{G_{cn}(s)}|$ and its upper bound $w_{uc}(s)$.

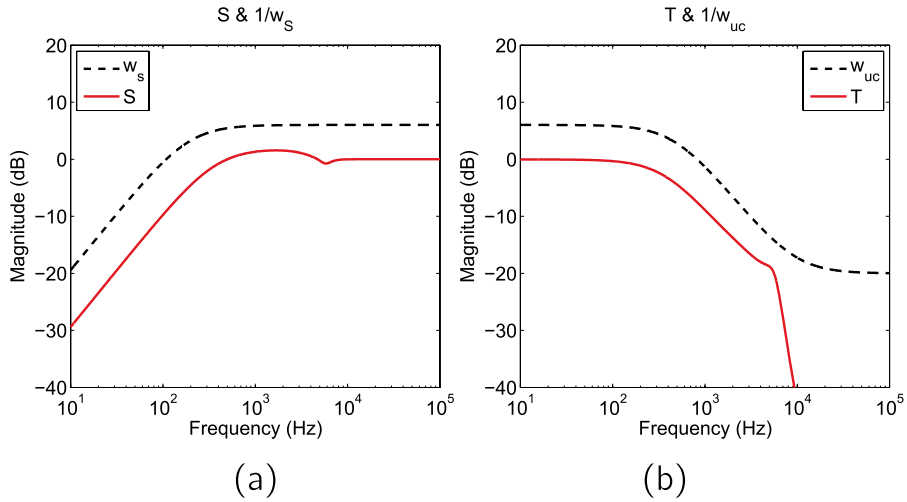

FIG. 10. The result of $\mathcal{H}_\infty$ synthesis. The control objective stated in (13) is satisfied as $|S| < |\frac{1}{w_s}|$ and $|T| < |\frac{1}{w_{uc}}|$.

in MFP3D. The robust control $K_\infty(s)$ has higher gain than PI control $K_{PI}(s)$ and is shaped around the frequencies where the dynamics of piezo and tip-sample interaction are important as shown in Figure 11.

Both controls are compared on the imaging of rectangular calibration grating. The experimental imaging with scan speed of 25 μm/s is shown in Figure 12 and 50 μm/s in Figure 13. A significant increase in the robustness to disturbances in the H_∞ control when compared to the PI control is evidenced in Figures 12(a), 12(c) and 13(a), 13(c). The image aberration at the bottom of Figures 12(a) and 13(a) is due to undesirable cantilever oscillations induced by disturbances that the PI control is unable to compensate for. These are not observed in Figures 12(c) and 13(c) since H_∞ control is designed to reject disturbances in that frequency range.

Since silicon oxide calibration grating has rectangular shape, it works like step response in sample height and results in large overshoot for $\mathcal{H}_\infty$ controller which has higher gain in high frequencies as shown in Figure 11.

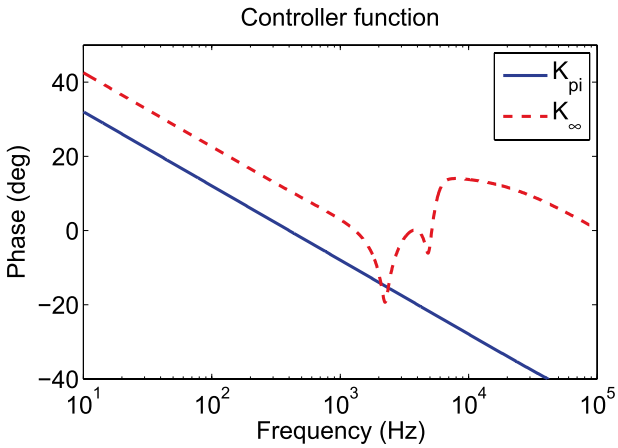

FIG. 11. Comparison of PI and $\mathcal{H}_\infty$ controller functions. The $\mathcal{H}_\infty$ controller considers the dynamics of vertical piezo-positioner and the tip sample interaction model.

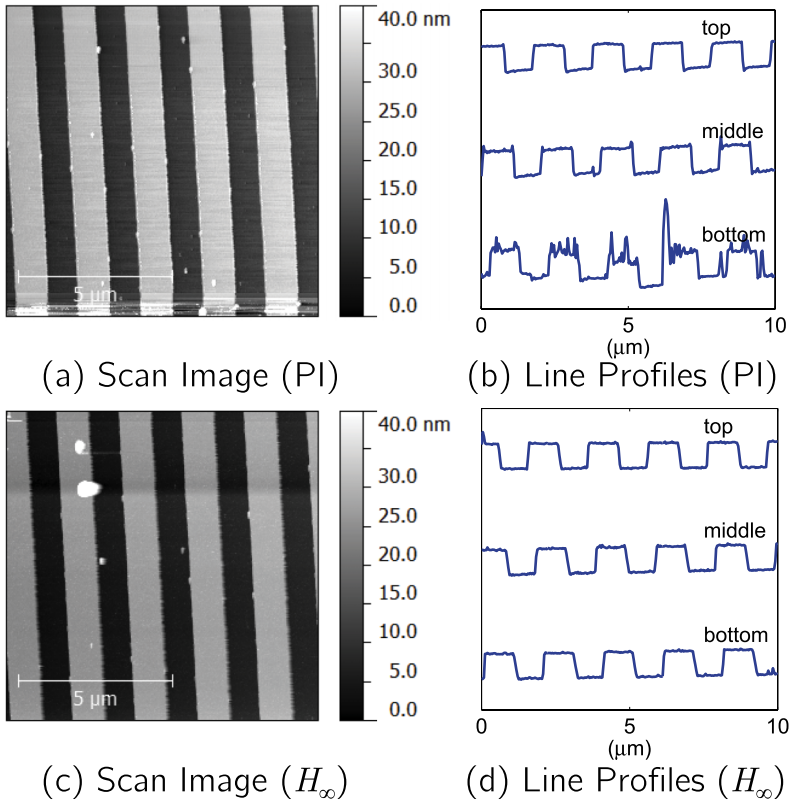

FIG. 12. Height estimate of PI and $\mathcal{H}_\infty$ controls at 25 μm/s scanning of 10 μm range in NGR22010 calibration grating. The bottom part of scan image is where AFM starts scanning and large disturbance acts on. PI control shows large oscillation in (a) and (b), but $\mathcal{H}_\infty$ control shows clear images (c) and (d) because it is designed to consider the tip-sample interaction with uncertainty.

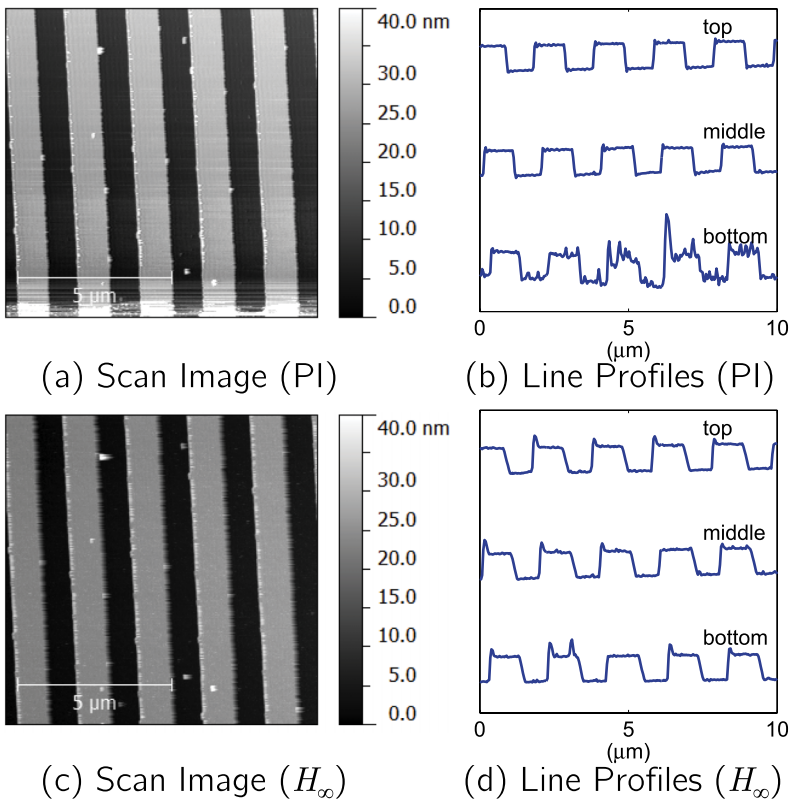

FIG. 13. Height estimate of PI and $\mathcal{H}_\infty$ controls at 50 μm/s. Similarly to the slower case, oscillation in PI control is large when scanning starts, but it does not occur in $\mathcal{H}_\infty$ case.

C. Discussion about PI and $\mathcal{H}_\infty$ control

According to the linear system analysis based on nominal models, -3dB imaging bandwidths of PI and $\mathcal{H}_\infty$ controls are 81 Hz (PI) and 256 Hz ($\mathcal{H}_\infty$), and $\|S\|_\infty$ which is the measure of robustness in control system is 1.20 (PI) and 1.18 ($\mathcal{H}_\infty$), respectively. $\|S\|_\infty$ of PI control is also considerably low in general linear control design. However, if P or I gains increased in experiment, then the control becomes unstable and is vulnerable to external disturbance. This stems from the fact that since the nonlinear $a - \phi$ dynamics is linearized, analysis can deviate from linear system framework. Even though linearized dynamics allows for a control design that does give better performance, all the analysis do not translate into experiments. The $\mathcal{H}_\infty$ control which has higher gain and broad bandwidth can be more robust since it specifically accounts for the tip-sample interaction model uncertainties and external disturbance.

VII. CONCLUSIONS

In this study, the model based robust control approach for achieving high bandwidths in dynamic-mode AFM is presented. Asymptotic perturbation techniques were used for modeling and control design for dynamic mode AFM. Through asymptotic perturbation and linearization about the equilibrium, the tip-sample interaction can be posed as linear model with large uncertainties. A control design based on robust control tools is developed that aims at achieving performance (amplitude set point tracking) while guaranteeing robustness to the modeling uncertainties.Experimental results from AFM imaging show a higher robustness of the imaging to disturbances and imaging bandwidth with the H_∞ design compared to PI designs.

[1]G. Binnig, C. F. Quate, and C. Gerber, Phys. Rev. Lett. **56**, 930 (1986).
[2]M. Gauthier, N. Sasaki, and M. Tsukada, Phy. Rev. B **64**, 085409 (2001).
[3]T. Sulchek, G. G. Yaralioglu, C. F. Quate, and S. C. Minne, Rev. Sci. Instrum. **73**, 2928 (2002).
[4]R. García and R. Pérez, Surf. Sci. Rep. **47**, 197 (2002).
[5]F. Giessibl, Rev. Mod. Phys. **75**, 949 (2003).
[6]N. Kodera, M. Sakashita, and T. Ando, Rev. Sci. Instrum. **77**, 083704 (2006).
[7]P. Agarwal, T. De, and M. V. Salapaka, Rev. Sci. Instrum. **80**, 103701 (2009).
[8]C. Lee and S. M. Salapaka, Appl. Phys. Lett. **97**, 133101 (2010).
[9]T. R. Rodríguez and R. García, Appl. Phys. Lett. **80**, 1646 (2002).
[10]C. Lee, "Control-systems based analysis and design methos for scanning probe microscopy," Ph.D. thesis (University of Illinois at Urbana-Champaign, 2010).
[11]J. N. Israelachvili, *Intermolecular and Surface Forces* (Academic Press, 1985).
[12]B. Bhushan, *Handbook of Micro/Nano Tribology*, 2nd ed. (CRC Press, 1999), p. 289.
[13]L. Wang, Appl. Phys. Lett. **73**, 3781 (1998).
[14]R. García and A. San Paulo, Phys. Rev. B **60**, 4961 (1999).
[15]S. Salapaka, M. Dahleh, and I. Mezic, Nonlinear Dyn. **24**, 333 (2001).
[16]S. Hu and A. Raman, Phys. Rev. Lett. **96**, 036107-1 (2006).
[17]N. Sasaki and M. Tsukada, Appl. Surf. Sci. **140**, 339 (1999).
[18]A. Sebastian, A. Gannepalli, and M. Salapaka, in *Proceedings of the 2004 American Control Conference*, Boston, Massachusetts, 2004 (IEEE, 2004), Vol. 3, pp. 2499–2504.
[19]N. N. Bogoliubov and Y. A. Mitropolskii, *Asymptotic Methods in the Theory of Non-linear Oscillations* (Gordan and Breach, New York, 1961).
[20]A. Nayfeh, *Perturbation Methods* (Wiley, New York, USA, 1973).
[21]J. Awrejcewicz, *Asymptotic Approaches in Nonlinear Dynamics: New Trends and Applications* (Springer, Berlin, 1998).
[22]S. Skogestad and I. Postlethwaite, *Multivariable Feedback Control, Analysis and Design*, 2nd ed. (John Wiley and Sons, 2005).
[23]P. Ge and M. Jouaneh, IEEE Trans. Control Syst. Technol. **4**, 209 (1996).
[24]D. Croft, G. Shedd, and S. Devasia, J. Dyn. Syst., Meas., Control **123**, 35 (2001).
[25]M. Rakotondrabe, Y. Haddab, and P. Lutz, in *ICARCV '06. 9th International Conference on Control, Automation, Robotics and Vision, 2006* (IEEE, 2006), pp. 1–8.